J Mater Sci: Mater Electron (2017) 28:6131–6137
DOI 10.1007/s10854-016-6291-6

Glass structure of the $CaO–B_2O_3–SiO_2–Al_2O_3–ZnO$ glasses system with different Si content

Jiao Han[1] · Yuanming Lai[1,2] · Yao Xiang[1] · Shuang Wu[1] · Ying Xu[1] · Yiming Zeng[1] · Jialin Chen[1] · Jisong Liu[1]

Received: 19 October 2016 / Accepted: 23 December 2016 / Published online: 4 January 2017

Abstract The aim of the present work is to investigate the effects of SiO_2 content on the structure of $CaO–B_2O_3–SiO_2–Al_2O_3–ZnO$ glass using the MAS-NMR, the fourier transform infrared spectrometer and differential scanning calorimetry (DSC). The results showed that the majority of Al existed in fourfold coordination and Zn acted as glass modifier in glass structure. With the increasing of SiO_2 content, the relative amount of B^{III} units decreased while the B^{IV} units increased and the proportion of Si–O–Si bridge oxygen bond in $[SiO_4]$ tetrahedrons increased obviously. The DSC curves revealed that the glass transition temperature increased from 732 to 773 °C with the increasing of SiO_2 content, indicating that SiO_2 generating more bridge oxygen can increase the degree of polymerization of glass structure.

1 Introduction

Borosilicate glass has attracted a subject of widespread interest in a number of fields and been extensively used for technical applications over the years, from the high emissivity coating materials [1] to the optical glasses for smart windows applications [2], or as biofilms to treat and recurrent infections [3], or also for storage of nuclear waste for its excellent properties [4] and electronic glasses in low temperature co-fired ceramics (LTCC) technology [5].

In order to get more suitable properties for the applications, the structure and composition of calcium borosilicate glass ($CaO–B_2O_3–SiO_2$, CBS) are carefully tailored to obtain the desired crystallization and physical properties or dielectric properties of the glass. Lai et al. [6] investigated the structure of CBS glasses with varying Si/Ca ratios (with constant Si/B value), which revealed that the structural units, like as the BO_3, BO_4 units and Si–O–Si units, determined the physical properties of glasses. In addition, the introduction of oxide in borosilicate glass could be an effective way to change structure of glass and then optimize the nature of the glass [7, 8]. Liu et al. [9] investigated the effects of Al_2O_3 on the structure and crystallization of $CaO–B_2O_3–SiO_2$ glass. The results revealed that the bending and stretching vibrations in $[SiO_4]$ units became weak with the increasing the Al_2O_3 content, CBS glass ceramics sample with 5 wt% Al_2O_3 achieved the best sintering characterization and dielectric properties ($\varepsilon_r \approx 7$, tan $\delta = 1.9 \times 10^{-3}$ at 1 MHz). Also, LaComb et al. [8] utilized ^{11}B, ^{17}O, and ^{27}Al NMR studied several calcium aluminosilicate glasses, which have demonstrated clear distinction among resonances for ^{17}O associated with boron and/or aluminum, including quantification of NBO associated with boron, aluminum and silicon in these multicomponent glasses. All of the above researches showed that the presence of high-coordinated Al species in aluminosilicate glasses can modify the structure and should be taken into account for glass structural optimization (Al distribution, Si/Al disorder for instance).

In addition, the structure of borate glass containing ZnO has drawn much attention due to its role in the

✉ Jiao Han
hanjiao90@sina.com

✉ Yiming Zeng
zengym0871@126.com

[1] State Key Laboratory of Advanced Technologies for Comprehensive Utilization of Platinum Metals, Kunming Institute of Precious Metals, 650106 Kunming, People's Republic of China

[2] State Key Laboratory of Electronic Thin Films and Integrated Devices, University of Electronic Science and Technology of China, 610054 Chengdu, People's Republic of China

glass structure as a modifier or network former based on its content [10, 11]. Colak et al. [12] have concluded that the amount of ZnO in borate glass structure has a dramatic effect on the number of non-bridging oxygen atoms that determine the role of ZnO as a modifier/network former. ZnO acted as a network former when having more than 5% (weight%) ZnO in samples, the opposite was modifier. Park et [13]. designed the calcium zinc borosilicate glass to achieve high thermal expansion for low temperature co-firing ceramic applications. The $50CaO–20ZnO–20B_2O_3–10SiO_2$ glass demonstrated CTE of 12.8 10^{-6}/K and dielectric constant of 13.5, and when it mixed with 50 wt% Al_2O_3 and sintered at 875 °C for 2 h, the glass–alumina composites demonstrated 95.5% of the relative density, indicating the feasibility for the application in LTCC materials with high CTE. Based on the above analysis, Al_2O_3 and ZnO played an important role in the structure and properties of $CaO–B_2O_3–SiO_2$ glass.

Therefore, we designed the $CaO–B_2O_3–SiO_2–Al_2O_3–ZnO$ glass composition. Besides, the SiO_2 content as network former is vital to the structure and properties of glass. Considering the above factors, in this paper, we presented a detailed report on the structures and characteristic temperature of $CaO–B_2O_3–SiO_2–Al_2O_3–ZnO$ glass with different SiO_2 content utilizing ^{11}B, ^{27}Al and ^{29}Si NMR, fourier transform infrared spectrometer(FT-IR) measurement and differential scanning calorimetry (DSC), especially the relationship between the SiO_2 content and the existence units of glass component in the glass network, which will point a robust approach for the study of the structure of glass.

2 Experimental work

2.1 Preparation of glass samples

The CS ($40CaO–30SiO_2–15B_2O_3–10Al_2O_3–5ZnO$, mol%) + $xSiO_2$ glasses, where $x = 0$, 5, 10, 15 and 20 wt%, were prepared using analytically pure $CaCO_3$, H_3BO_3, SiO_2, Al_2O_3 and ZnO as the starting materials. The experimental glasses were named as CS_0, CS_5, CS_{10}, CS_{15}, and CS_{20}, respectively. The procedure was as follows: we first weigh the CS composition based on the ratio of moles and mix it with SiO_2 to get the mixing powders, followed by transferring them into Pt crucibles for melting at a temperature of 1400 °C for 2 h in air. After melting, the melt was quickly quenched into deionized water to prevent the occurrence of any crystallization. The as-quenched glass was ground and screened through a 500-mesh stainless steel wire screen to obtain glass powders with particle size <25 μm.

2.2 Characterization of the samples

Fourier transform infrared spectrometer (FT-IR, Thermo Nicolet Smart-380) was carried out in the frequency range 400–2000 cm^{-1} at room temperature with a resolution of 1 cm^{-1} on glass powders. Samples for FT-IR measurements were prepared by mixing and grinding a small quantity of glass powder with spectroscopic grade dry KBr powder and then compressing the mixtures to obtain pellets for testing. A differential scanning calorimetry (DSC, STA409 PG/PC, Netzsch, Germany) was carried out in a flowing atmosphere of dry air from ambient temperature to 1000 °C with a heating rate of $\beta = 5$ °C/min to determine the glass transition temperature (T_g) and the crystallization behavior. The DSC experiments were carried out using alumina crucibles with a-Al_2O_3 powder as a reference material.

^{11}B, ^{27}Al and ^{29}Si magic angle spinning nuclear magnetic resonance spectroscopy (MAS-NMR, Varian Infinity-plus 400) were performed on glass samples. ^{11}B MAS spectra were acquired at 192.4 MHz using a Bloch decay sequence with a pulse width of 0.6 μs (ca. 13° tip angle). Recycle delays ranged from 5 to 15 s and 32 to 64 co-added transients were collected. All ^{11}B NMR spectra were referenced using 0.1 M H_3BO_3 (19.6 ppm relative to BF_3 OEt_2). ^{27}Al MAS spectra were acquired at 156.2 MHz using a Bloch decay sequence with a pulse width of 0.4 μs (ca. 12° tip angle). Collected transients ranged from 256 to 512 with recycle delays of 1 or 15 s. ^{27}Al spectra were referenced using 0.1 M $Al(H_2O)_6$ (0.0 ppm). For ^{29}Si MAS-NMR, the tetramethylsilane (−9.9 ppm) was used as the chemical shift reference. The spectrometer was operated at a Larmor frequency of 59.4 MHz with a 7.02 T magnetic field with a 4 mm CPMAS probe at a spinning frequency of 10 kHz. Spectra were obtained by a CPMG pulse sequence, which accumulating typically 32 echoes with a delay of 2–3 ms (consecutive 180° pulses with a 20 s recycle delay). The measurements were performed with a resolution of 0.1 ppm. Most part of the experimental errors came from the residual linewidth and the line shape both of which caused by the filed inhomogeneity and the sample nature. In characterization of this paper, we neglect the experimental errors due to the consistency of test conditions. In addition, the degree of fitting is more than 99.7% in the deconvolution for all elements.

3 Results and discussion

3.1 MAS-NMR spectroscopy

Figure 1a–c showed the ^{11}B, ^{27}Al and ^{29}Si MAS-NMR spectra of the experimental glasses, respectively. In all three figures, the spectra show relatively broad

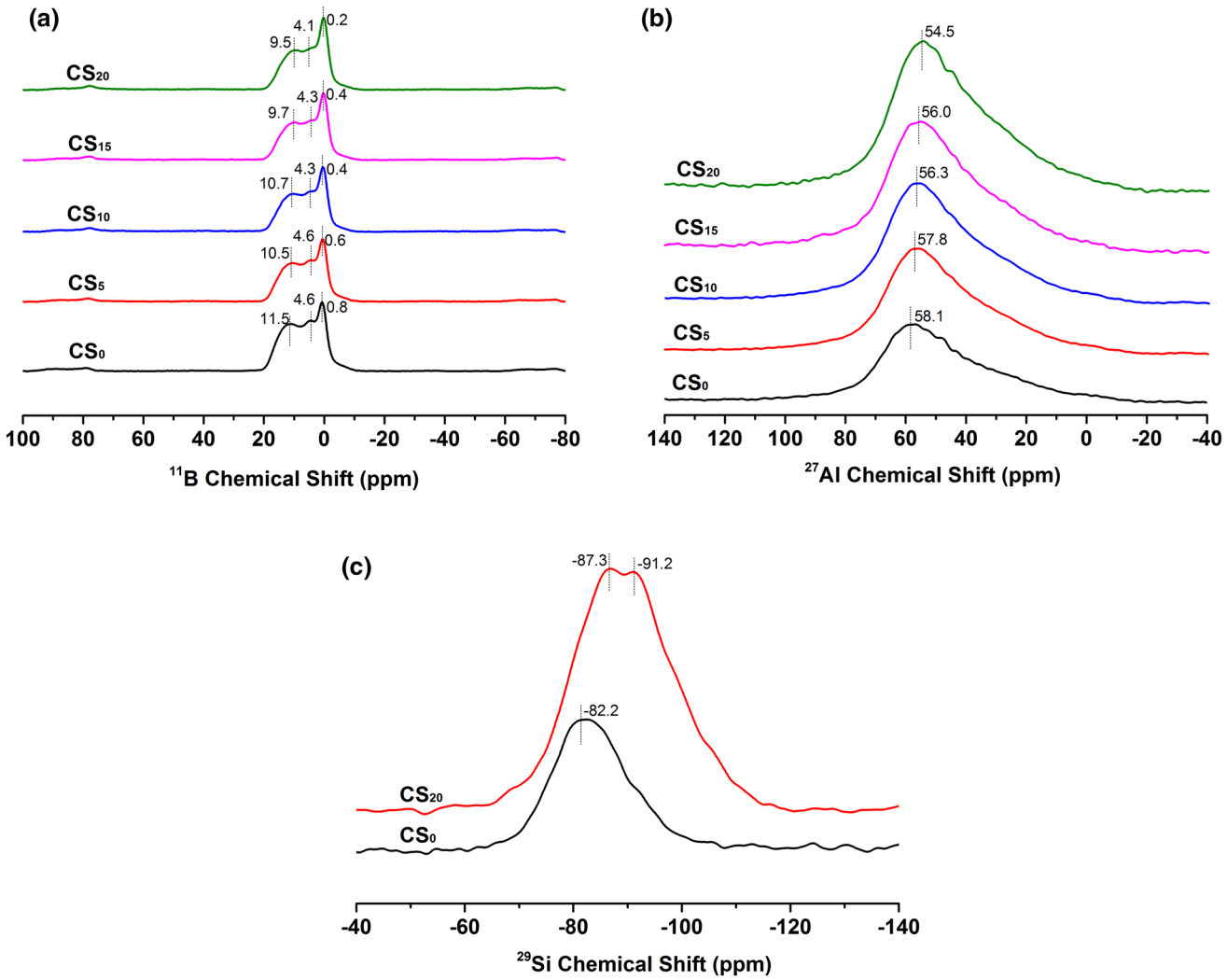

Fig. 1 NMR spectra of **a** ^{11}B, **b** ^{27}Al and **c** ^{29}Si of experimental glasses

peaks which are tell-tale features for glasses, revealing their amorphous nature and wide distributions of bond angles and bond lengths. From the ^{11}B MAS-NMR spectra in Fig. 1a, it can be seen that all glass samples have two broad peaks, in the range of 9.5–11.5 ppm and 4.6–4.1 ppm, which associated with trigonal [BO_3] (B^{III}) coordinated boron [14]. Another relatively sharper peak centered 0.2–0.8 ppm, corresponding to tetrahedral (BO_4, B^{IV}) boron species [15]. In order to quantitatively determine the fractions of B^{III} and B^{IV} units of boron, the ^{11}B MAS-NMR spectra were deconvoluted and the example of CS_0 was showed in Fig. 2a. Spectra were fitted with four peaks: the peaks at 12.93 ppm and 4.07 ppm are corresponding to asymmetric (B^{IIIa}, boron with 1 or 2 bridging oxygens) and symmetric trigonal (B^{IIIs}, boron with 0 or 3 bridging oxygens) boron units respectively [15]. And the peaks at 0.43 and −6.78 ppm represent [BO_4] units, which can be assigned to boron atoms in sites similar to those in the borosilicate mineral superstructures, danburite and reedmergnerite units, i.e. [$B(OB)(OSi)_3$] and [$B(OSi)_4$] respectively [16]. The isotropic chemical shift (δ_{iso}) and the relative contents of each boron species in the deconvolution of the spectra are presented in Table 1.

The ^{27}Al MAS-NMR spectra for all experimental samples were presented in Fig. 1b. The spectra all consist of a narrow peak centered at around +50 ppm, consistent with Al^{IV} [17]. Also, the peaks are significantly and asymmetrically broader, mainly on the lower shift, which indicates the presence of higher Al coordination [17]. In order to figure out the true distribution of different Al coordination for all samples, the spectral deconvolution was performed using Gaussian by fitting one line shape and an example of CS_0 was presented in Fig. 2b. The peaks having chemical shifts 57.16, 31.30 and 6.9 ppm can be attributed to Al^{IV}, Al^{V} and Al^{VI} species [18], respectively. And the relative amount of Al^{IV} unit is ~80% for all glasses, it can be concluded

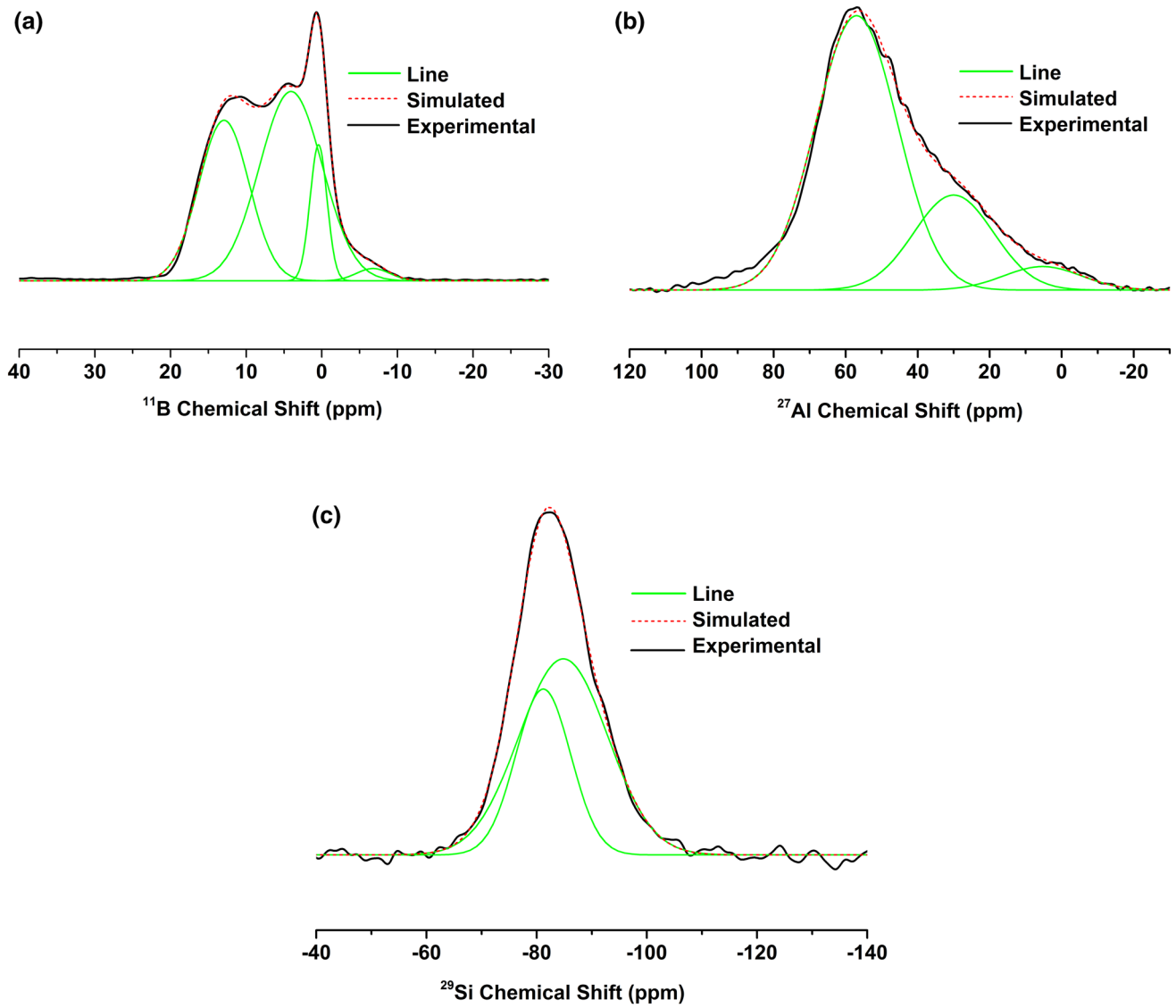

Fig. 2 Deconvolution of **a** ^{11}B, **b** ^{27}Al of CS_0 and **c** ^{29}Si nuclei of CS_{20} NMR spectra

that majority of Al exists in fourfold coordination in glass structure.

The ^{29}Si MAS-NMR spectra for CS_0 and CS_{20} were showed in Fig. 1c. From it we can see that the spectrum presents a peak maximum near 82 ppm for CS_0 and the other two peaks located in ~90 ppm for CS_{20}. Deconvolution of ^{29}Si spectra were performed in order to quantitatively determine the fractions of Si units present. An example of ^{29}Si deconvolution of CS_{20} sample is presented in Fig. 2c and the relative amounts of each Q unit as well as the fitting parameters are presented in Table 2. Deconvolution based on a Gaussian fit resulted in two peaks around ~81 and ~85 ppm in CS_0 sample, which are characteristic of the Q^2 and Q^3 structural units of silicon respectively (where Q^n represents silicon structural units having 'n' bridging oxygen atoms in [SiO_4] tetrahedron), while the peaks around ~88 and ~103 ppm in CS_{20} sample are attributed to the Q^3 and Q^4 units, respectively [15].

Based the above analysis, we have noticed that the peaks shift toward the lower frequency (Fig. 1a, b, c) with the increasing of SiO_2 content. According to the ^{11}B NMR spectral deconvolution (Fig. 2a; Table 1), B exists as B^{IV} and the rest is present as B^{III} units. With the increasing of SiO_2 content, the relative amount of B^{III} units decrease from 88.21 to 82.81%, while the B^{IV} units increase from 11.79 to 17.19%. Also, the variation of Q^n units (Table 2) shows that the relative amount of Q^2 unit is faded away from 65.73 to 0% while the Q^4 unit gradually appears form 0 to 9.23%, and the Q^3 unit increases from 65.73 to 90.77% for CS_0 and CS_{20} samples, respectively. The change

Table 1 NMR parameters for ^{11}B deconvolution

	Boron site	δ_{iso} (ppm)	Amount (%)	
CS_0	B^{IIIa}	12.96	34.89	88.21
	B^{IIIs}	4.12	53.32	
	B^{IV}(1B,3Si)	0.43	10.24	11.79
	B^{IV}(0B,4Si)	−6.76	1.55	
CS_5	B^{IIIa}	12.54	33.22	85.96
	B^{IIIs}	3.98	52.74	
	B^{IV}(1B,3Si)	0.30	12.86	14.04
	B^{IV}(0B,4Si)	−6.59	1.18	
CS_{10}	B^{IIIa}	12.05	36.13	84.64
	B^{IIIs}	3.64	48.51	
	B^{IV}(1B,3Si)	0.20	14.48	15.36
	B^{IV}(0B,4Si)	−6.29	0.88	
CS_{15}	B^{IIIa}	12.03	33.08	83.49
	B^{IIIs}	3.61	50.41	
	B^{IV}(1B,3Si)	0.05	15.48	16.51
	B^{IV}(0B,4Si)	−6.93	1.06	
CS_{20}	B^{IIIa}	11.71	33.38	82.81
	B^{IIIs}	3.39	49.43	
	B^{IV}(1B,3Si)	0.02	16.03	17.19
	B^{IV}(0B,4Si)	−7.16	1.16	

occurred in the shift of peaks, B units (B^{III} unit decreases while B^{IV} unit increases) and Q^n unit (Q^2 unit fades away, Q^3 unit increases and Q^4 unit gradually appears) is ascribed to the increasing of SiO_2 content, which will produce more bridging oxygens. The B^{III} units will connect bridging oxygens to form B^{IV} units, and the increase of bridging oxygens will result in the transformation of Q^{n-1} to Q^n unit [18], which can increase the polymerization degree of [SiO_4] tetrahedral. The increasing amount of boron, aluminium and silicon with bridging oxygens will make the peaks shift to lower frequency [19]. In addition, the increase in FWHM of Q^3 peak (Table 2) is possibly due to the wide distribution of bond lengths and bond angles due to the amount change of B^{III} and B^{IV} units.

3.2 The FT-IR analysis

Figure 3 presents the FT-IR spectra of CS_x glasses for x = 0, 5, 10, 15 and 20 between 400 and 2000 cm^{-1}. The results of FT-IR absorbance spectra show broad peaks indicating

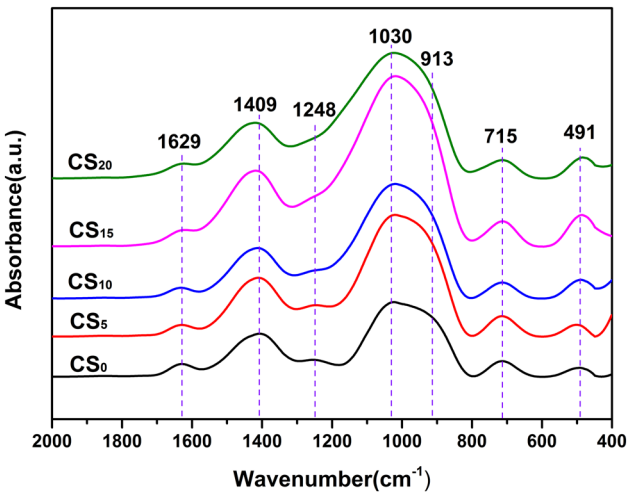

Fig. 3 The FT-IR spectra of the experimental glasses

the amorphous nature of the glasses and wide distribution of Q^n units. The glass compositions show seven absorption bands and these peak positions are assigned to various vibrational modes. The high frequency band at 1639 cm^{-1} can be assigned to the molecular water [20]. That band near 1409 cm^{-1} is characteristic of antisymmetric stretching vibration of [BO_3] [21], and its peak shifted to higher wavenumbers. The band at 1248 cm^{-1} is due to the B–O–B stretch vibration in [BO_3] [22], and its peak weakens with the SiO_2 content increasing, indicating that [BO_3] stretch vibration is subdued with the increasing of SiO_2. The result is consistent with the ^{11}B NMR displayed the decrease of B^{III} units (as shown in Table 1). The band located around 1029 cm^{-1} is attributed to superposition of asymmetric stretching vibration of Si–O–Si in [SiO_4] tetrahedron unit and B–O asymmetric stretching of tetrahedral [BO_4] unit [4], and the peak shifted to lower wavenumbers and the intensity increased obviously, indicating that more [BO_4] tetrahedron units appear with the increase of SiO_2 content generated more bridging oxygen. The results are accord with the analysis of ^{11}B MAS NMR spectra. In addition, the band of 913 cm^{-1} is due to B–O stretching in BO_4 units/Si–O–Si stretching [23]. The appeared band of 722 cm^{-1} is attributed to stretching vibrations of Al–O bond in [AlO_4]

Table 2 NMR parameters for ^{29}Si deconvolution

	δ_{iso} (ppm)			FWHM (ppm)			Amount (%)		
	Q^2	Q^3	Q^4	Q^2	Q^3	Q^4	Q^2	Q^3	Q^4
CS_0	−81.19	−84.83	–	11.68	18.96	–	34.27	65.73	–
CS_{20}	–	−88.33	−103.25	–	19.50	15.20	–	90.77	9.23

δ_{iso} chemical shift, *FWHM* full width at half maximum

tetrahedral [24] and the bending vibration of the B–O–B bonds in the borate network [24, 25]; the band located around 490 cm^{-1} is attributed to bending vibration of Si–O–Si and Al–O stretching vibrations in [AlO_6] octahedral [25, 26]. In general, the structure of glasses is formed by a network of BO_3 triangles, SiO_4 and AlO_4 tetrahedra with minor contribution of BO_4 tetrahedra. The Zn does not appear in the glass structure, which revealed ZnO acted as a modifier in glass samples having <5% (weight%) incorporation [12].

3.3 DSC analysis

Differential scanning calorimetric patterns corresponding to the experimental glasses containing different amounts of SiO_2 are shown in Fig. 4. All the patterns reveal that the glass is thermally stable up to 700 °C. The glass transition temperatures (T_g) are obtained from the onset of slope change of the DSC curves. The curves exhibit typical glass transitions with the inflection point between 730 and 780 °C. The glass transition temperature is 732, 735, 749, 767 and 773 °C for samples CS_0, CS_5, CS_{10}, CS_{15} and CS_{20} respectively. This may be the results that SiO_2 acts as a network former and causes densification of the glass structure, making the polymerization degree of glass structure increase with the addition of SiO_2. Also, the melting point of SiO_2 is higher than other components in glass raw material. Both of which will cause the glass transition temperatures to rise with the increasing of SiO_2 content. In addition, sample CS_0 shows two weak crystallization peaks, related to the formation of the crystalline phase of wollastonite [27] and borocalcite [28], respectively. With the increasing of SiO_2 content, it should be noted that crystallization peaks are completely absent in the DSC traces of other glasses. This may be due to the fact that the densification of glass structure will make the crystallization activation energy increase so that the wollastonite and borocalcite phases appear difficultly. Therefore, the increasing of SiO_2 content in glasses seems to stabilize these glasses, which show no tendency towards crystallization on heating.

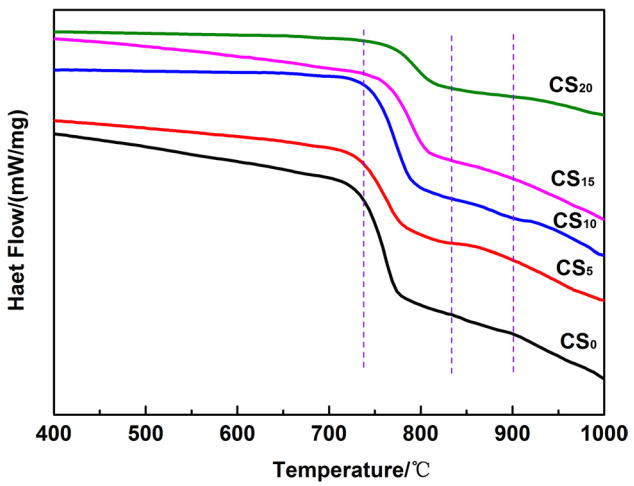

Fig. 4 DSC curve of the experimental glasses

4 Conclusions

The current study using MAS-NMR, FT-IR and the density measurement technology investigated the role of SiO_2 content on $CaO–B_2O_3–SiO_2–Al_2O_3–ZnO$ glasses structure. The absence of Zn-related units for all glasses calls to mind the idea of ZnO acting as a modifier due to its incorporation under 5% (weight%) in glasses. Al mainly goes in to the glass network in fourfold coordination and few five, sixfold coordination whereas B goes in as both four and threefold coordination, and the relative amount of B^{III} units decrease while the B^{IV} units increase with the increasing of SiO_2 content. Also, the relative amount of Q^2 unit is faded away while the Q^4 unit gradually appears and the Q^3 unit increases in [SiO_4] tetrahedrons with the increase of SiO_2 content. In addition, the increase of the glass transition temperatures (T_g) for all glass compositions suggests that SiO_2 acts as a network former and causes densification of the glass structure.

Acknowledgements The authors thank the National Center for Magnetic Resonance in Wuhan acquiring the MAS-NMR measurement. This work was supported by the fund of the State Key Laboratory of Advanced Technologies for Comprehensive Utilization of Platinum Metals (Nos. SKL-SPM-201535, 201548), The 551 project of Kunming, the Basic Applied Research Foundation of Yunnan Province, China (Grant Nos. 2016FD125, 2016FB083) and Science &Technology Program of Yunnan Province (No. 2014DC019).

References

1. G. Shao, X. Wu, Y. Kong, X. Shen, S. Cui, X. Guan, C. Jiao, J. Jiao, J. Alloy Compd. **663**, 360 (2016)
2. M.Y. Hassaan, H.M. Osman, H.H. Hassan, A.S. El-Deeb, M.A. Helal, Ceram. Int. (2016). doi:10.1016/j.ceramint.2016.10.137
3. M. Klinger-Strobel, O. Makarewicz, M.W. Pletz, A. Stallmach, C. Lautenschlager, J. Mater. Sci. **27**, 175 (2016)
4. M. Sitarz, J. Non-Cryst. Solids **357**, 1603 (2011)
5. M. Ma, Z. Liu, F. Zhang, F. Liu, Y. Li, R. Bordia, J. Am. Ceram. Soc. **99**, 2402 (2016)
6. Y. Lai, Y. Zeng, X. Tang, H. Zhang, J. Han, H. Su, RSC Adv. **6**, 93722 (2016)
7. S. Khan, G. Kaur, K. Singh, Ceram. Int. **43**, 722 (2017)
8. M. LaComb, D. Rice, J.F. Stebbins, J. Non-Cryst. Solids **447**, 248 (2016)
9. J.Z. Liu, X.F. Wu, N.X. Xu, Q.L. Zhang, H. Yang, J. Mater. Sci. **26**, 8899 (2015)

10. T.R. Rao, C.V. Reddy, C.R. Krishna, U.S.U. Thampy, R.R. Raju, P.S. Rao, R.V.S.S.N. Ravikumar, J. Non-Cryst. Solids **357**, 3373 (2011)
11. R. Stefan, E. Culea, P. Pascuta, J. Non-Cryst. Solids **358**, 839 (2012)
12. S. Cetinkaya Colak, I. Akyuz, F. Atay, J. Non-Cryst. Solids **432**, 406 (2016)
13. J.S. Park, Y. Kim, H. Shin, J.H. Moon, W. Lim, J. Am. Ceram. Soc. **91**, 3630 (2008)
14. K. Herzog, J. Peters, B. Thomas, C. Jäger, Ber. Bunsenges. Phys. Chem **100**, 1655 (1996)
15. A. Gaddam, H.R. Fernandes, J.M.F. Ferreira, RSC Adv. **5**, 41066 (2015)
16. B.G. Parkinson, D. Holland, M.E. Smith, A.P. Howes, C.R. Scales, J. Phys. **19**, 415114 (2007)
17. S.H. Risbud, R.J. Kirkpatrick, A.P. Taglialavore, B. Montez, J. Am. Ceram. Soc. **70**, C-10(1987)
18. S. Sen, Z. Xu, J. Stebbins, J. Non-Cryst. Solids **226**, 29 (1998)
19. A. Saini, A. Khanna, V.K. Michaelis, S. Kroeker, F. González, D. Hernández, J. Non-Cryst. Solids **355**, 2323 (2009)
20. K. Singh, I. Bala, V. Kumar, Ceram. Int. **35**, 3401(2009)
21. A. Aronne, S. Esposito, P. Pernice, Phys. Chem. Glasses **40**, 63 (1999)
22. X. Zhu, C. Mai, M. Li, J. Non-Cryst. Solids **388**, 55 (2014)
23. M. Nakamura, Y. Mochizuki, K. Usami, Y. Itoh, T. Nozaki, Solid State Commun. **50**, 1079 (1984)
24. N. Santha, T. Nideep, S. Rejisha, J. Mater. Sci. **23**, 1435 (2012)
25. G.J. Mohini, N. Krishnamacharyulu, G. Sahaya Baskaran, P.V. Rao, N. Veeraiah, Appl. Surf. Sci **287**, 46 (2013)
26. H. Shao, H.Q. Zhou, X.D. Shen, Adv. Mater. Res. **189**, 4466 (2011)
27. J.H. Jean, C.R. Chang, C.D. Lei, J. Am. Ceram. Soc. **87**, 1244 (2004)
28. C.R. Chang, J.H. Jean, J. Am. Ceram. Soc. **82**, 1725 (1999)